Toward a Better Understanding of the Poly(glycerol sebacate)–Water Interface

Xavier Davoy, Julien Devémy, Sébastien Garruchet, Alain Dequidt, Patrice Hauret, Patrice Malfreyt

Towards a better understanding of the Poly(Glycerol Sebacate) (PGS)-water interface

Xavier Davoy,*,†,‡ Julien Devémy,† Sébastien Garruchet,‡ Alain Dequidt,† Patrice Hauret,‡ and Patrice Malfreyt*,†

†*Université Clermont Auvergne, CNRS, Clermont Auvergne INP, Institut de Chimie de Clermont-Ferrand, F-63000 Clermont-Ferrand, France*
‡*Manufacture Française des Pneumatiques Michelin, 23 Place des Carmes, Clermont-Ferrand, 63040, France*

E-mail: Xavier.Davoy@uca.fr; Patrice.Malfreyt@uca.fr

Abstract

Molecular simulations were conducted to provide a better description of the poly(glycerol sebacate) (PGS)-water interface. The density and the glass transition temperature as well as their dependencies on the degree of esterification were examined in close connexion with available experimental data. The work of adhesion and water contact angle were calculated as a function of the degree of esterification. A direct correlation was established between the strength of the hydrogen bond network in the interfacial region and the change of the water contact angle with respect to the degree of esterification. The interfacial region was described by local density profiles and orientations of water molecules.

Introduction

Poly(glycerol sebacate) (PGS) is a biodegradable and bioresorbable elastomer formed through the polycondensation of glycerol and sebacic acid. Both reactants of the synthesis of PGS are endogenous monomers that are present in human metabolites. More specifically, glycerol, a basic building bock for lipids, is involved in the synthesis of phospholipids and sebacic acid is a natural metabolite in fatty acid oxidation.[1,2] These two monomers were also approved by the US Food and Drug Administration (FDA). PGS was first obtained[3] in 2002 by Wang et al. with a three dimensional cross-linked structure[3] composited by equimolar of glycerol and sebacate acid. Since then, numerous works have been carried out with a view to optimizing the PGS synthesis and its properties.[4] Its favorable combination of properties[5] such as toughness,[3] good flexibility,[6] biocompatibility,[7] shape-memory[8] along with the fact that it degrades by surface erosion[9,10] into non-toxic products makes PGS as a good candidate for drug delivery,[11–13] tissue engineering[14–16] and diverse other biomedical applications.[5,17–19]

Physico-chemical and biological properties[4] of PGS-based systems were found to be dependent on the synthesis protocol,[20–25] morphology,[26] monomers ratio,[3,27,28] curing time,[29,30] crosslinking density[3,18,24,29] and temperature.[31] Additionally, an in-depth understanding of the interaction between PGS and water is critical for biocompatibility and biodegradability of materials in tissue engineering[32,33] and drug delivery.[34,35]

For example, the glass transition temperature T_g of PGS which is critical property to

inform us about the strength of the material, was measured under different conditions and operating methods. As the glycerol and sebacic acid molecular ratio changed from 2:2.5 to 2:4, the glass transition temperature[36] decreased slightly from 248 K to 241 K. Cai and Liu reported a T_g of 236 K for a PGS[8] cured at 393 K for 48 h. This thermal property was found equal[37] to 248 K for a PGS cured at the same temperature of 393 K for 96 h. For a slightly cross-linked PGS,[38] the glass transition temperature was measured at 255 K. T_g was found to range from 238 to 253 K under relatively mild curing conditions.[24] Very interestingly, recent experiments[30] have reported the glass transition temperature at different curing times and established that T_g was between 248 K and 268 K. In addition, Wu et al. showed no obvious direct link between the esterification degree and the glass transition temperature.[30] This lack of correlation between these two properties was already observed previously.[31]

Since water is the biological medium supporting the cellular activity, a poor affinity between water and PGS-based materials can limit a wider application in tissue engineering. The surface hydrophilicity[39] can be characterized by angle measurement.[30,36,40–42] PGS with a lower contact angle is more hydrophilic. Experiments[36] showed that the contact angle increased from 45° to 57° with increasing sebacic acid content ranging from 2.5 to 4 with 2 glycerol molecules in line with the increasing contributions of hydrophobic interactions due to the alkyl chains.[36] A recent study reported a contact angle of PGS about 95° whereas Aghajan et al. have measured a contact angle[42] of 73° for a PGS cured at 393 K for 48 h. Recently, the dependence of the contact angle on the curing time[30] was proposed for a PGS prepared at 403 K. The experimental data showed that water contact angle increased almost linearly with curing time ranging from 62° to 98° as curing time changed from 36 h to 96 h. This last result would show that the hydrophilicity of PGS decreases with increasing degree of cross-linking resulting in a reduction of the hydrophilic nature of the surface of PGS due to a modification in the hydrogen bond network in the PGS-water interface.[43] However, this molecular aspect has yet to be demonstrated.

These experimental studies reveal a certain disparity in the values of glass transition temperature and water contact angle underlining the effects of curing time and experimental conditions on the final properties of the PGS-based materials. However, it is essential to control these parameters to design PGS with tunable properties.[44] Additionally, bearing in mind that the formation of the three-dimensional polymer network changes gradually during the curing, it is also important to have an idea about the progressive change of the material upon the crosslinking process during the reaction. A key issue is how to achieve a high degree of esterification while maintaining a very good affinity of PGS with water as required for a biopolymer.

Controlling these parameters, which can influence the final properties of PGS-based materials but are difficult to access experimentally, is a major challenge in the design of these biomaterials. Such an approach can be achieved by using molecular simulation[45] which has the advantage of describing the material on a molecular scale and providing energy quantities using statistical thermodynamics. We applied molecular simulations to investigate macroscopic properties such as density, glass transition temperature and surface tension of epoxy resins as a function of the crosslinking degree for various prepolymers and hardeners.[46–48] To our knowledge, no molecular simulation has been carried out on PGS and its interaction with water. Only, finite element simulations[15] were carried out to predict the PGS curing conditions and scaffold effective stiffnesses. However, this computational modeling does not provide any information on interactions at the molecular level and on the structure-property relationship arising from the molecular and macroscopic scales.

We propose here to investigate the properties of a PGS-based material characterized by the stoichiometric ratio of 2:3 glycerol to sebacic acid molecules[49] by using molecular dynamics (MD) simulations. In a first step, we investigate the change in the formation of the polymer network by following the percolation pro-

cess and determining the gel point.[50] To evaluate the quality of the force field, we test it on the reproduction of the experimental density and the glass transition temperature. We also study the impact of the degree of esterification on these two properties. The interaction of the PGS with water is investigated through the calculation of the work of adhesion at various degrees of esterification. From the work of adhesion, it is possible to deduce the water contact angle at a given degree of esterification. We also calculate the number of hydrogen bonds between water and PGS that we correlate to the water contact angle. We complete this study by analyzing the arrangements of water molecules at the surface of PGS.

This paper is organized as follows. Section 2 describes the computational procedures in terms of potential models, method of simulation, calculation of work of adhesion and the creation of the polymer network. Section 3 discusses our main results and Section 4 contains our conclusions.

Model and methods

Model

Sebacic acid and glycerol molecules (see Figure 1) were modeled by using the OPLS-AA force field.[51–53] This molecular model sums intramolecular and intermolecular energy contributions to give the total configurational energy. The intramolecular interactions consist of bonds stretching, angle bending, dihedral and non-bonded energy contributions as described in Eq.(1).

$$U_{\text{intra}} = U_{\text{bonds}} + U_{\text{angles}} + U_{\text{torsions}} + U_{\text{nb}} \quad (1)$$

The bond stretching and angle bending energy are described by harmonic potentials defined by Eqs.(2) and (3), respectively.

$$U_{\text{bonds}} = \sum_i k_{\text{b},i}(r_i - r_{0,i})^2 \quad (2)$$

$$U_{\text{angle}} = \sum_i k_{\theta,i}(\theta_i - \theta_{0,i})^2 \quad (3)$$

In these equations, k_{b} and k_θ are the force constants and r_0 and θ_0 are equilibrium bond and angles values, respectively.

$$U_{\text{torsion}} = \frac{1}{2}\sum_i \Big(V_{1,i}(1+\cos\phi_i) + V_{2,i}(1-\cos 2\phi_i) + V_{3,i}(1+\cos 3\phi_i) + V_{4,i}(1-\cos 4\phi_i) \Big) \quad (4)$$

where ϕ is the dihedral angle and V_1, V_2, V_3 and V_4 are the Fourier coefficients of each dihedral angle.

Atoms separated by 1 or 2 bonds in the same molecules interact through the bonded potential only ($U_{\text{nb}} = 0$). As required by the OPLS force field, atoms separated by 3 bonds interact through the bonded potential plus half of the non-bonded interaction ($U_{\text{nb}} = 0.5\,U_{\text{inter}}$). Beyond 3 bonds, the atoms in the same molecule interact with the non-bonded interactions U_{inter} as if they belonged to different molecules. These non-bonded interactions sum dispersion-repulsion and electrostatics contributions, as written in Eq. (5).

$$U_{\text{inter}} = U_{\text{elect}} + U_{\text{LJ}} \quad (5)$$

The electrostatic interactions between two charges q_i and q_j at a distance r_{ij} is represented by the Coulomb potential as

$$U_{\text{elect}} = \sum_{i=1}^{N-1}\sum_{j=i+1}^{N} \frac{q_i\,q_j}{4\pi\,\epsilon_0\,r_{ij}} \quad (6)$$

where ϵ_0 represents the dielectric constant of the vacuum. The long range electrostatic interactions can be calculated by using the Particle-Particle Particle-Mesh (PPPM)[54] algorithm. This method computes electrostatic interactions by splitting the pair potential into two parts, the so-called real-space part is computed in a normal pairwise fashion and the so - called reciprocal-space is evaluated by using the Fourier transform.

The van der Waals interactions are mostly described by the 12-6 Lennard-Jones (LJ) potential as

$$U_{\mathrm{LJ}} = \sum_{i=1}^{N-1} \sum_{j=i+1}^{N} 4\varepsilon_{ij} \left[\left(\frac{\sigma_{ij}}{r_{ij}} \right)^{12} - \left(\frac{\sigma_{ij}}{r_{ij}} \right)^{6} \right] \quad (7)$$

where ε_{ij} ($\mathrm{kJ\,mol^{-1}}$) and σ_{ij} (Å) correspond to the energy parameter of the interaction and the Lennard-Jones core diameter. The non-bonded interactions are truncated by using a cutoff radius $r_c = 12\,\text{Å}$. The water molecules were modelled by using the SPC/E model.[55] The LJ parameters for the interactions between unlike sites were calculated by using the Lorentz-Berthelot combing rules[56,57] which are geometric for $\varepsilon_{ij} = (\varepsilon_{ii}\,\varepsilon_{jj})^{1/2}$ and $\sigma_{ij} = (\sigma_{ii}\,\sigma_{jj})^{1/2}$. The association of the OPLS-AA model with the SPC/E water model, has already been investigated on free energy of solvation of organic molecules.[58] A quantitative agreement with experimental data was also established.[58] Additionally, the SPC/E model was found to reproduce accurately the surface tension of water.[59,60]

Work of adhesion

The work of adhesion W_{SL} per unit of area of the solid-liquid interface is defined as the reversible thermodynamic work needed to separate the solid-liquid interface from the equilibrium state of two coexisting phases into two bulk phases that no longer interact at a separation distance of infinity.[61]

$$W_{\mathrm{SL}} = \gamma_{\mathrm{LV}} + \gamma_{\mathrm{SV}} - \gamma_{\mathrm{SL}} \quad (8)$$

where γ_{SL}, γ_{SV} and γ_{LV} are the solid-liquid, solid-vapor and liquid-vapor surface tensions, respectively.

The calculation of W_{SL} can be performed by using the concept of Free Energy Perturbation (FEP).[62–65] We then consider that the potential energy U of the system as a function of a coupling parameter λ such that $0 \leq \lambda \leq 1$. The simplest choice for the dependence of the energy on the coupling parameter is a linear function as

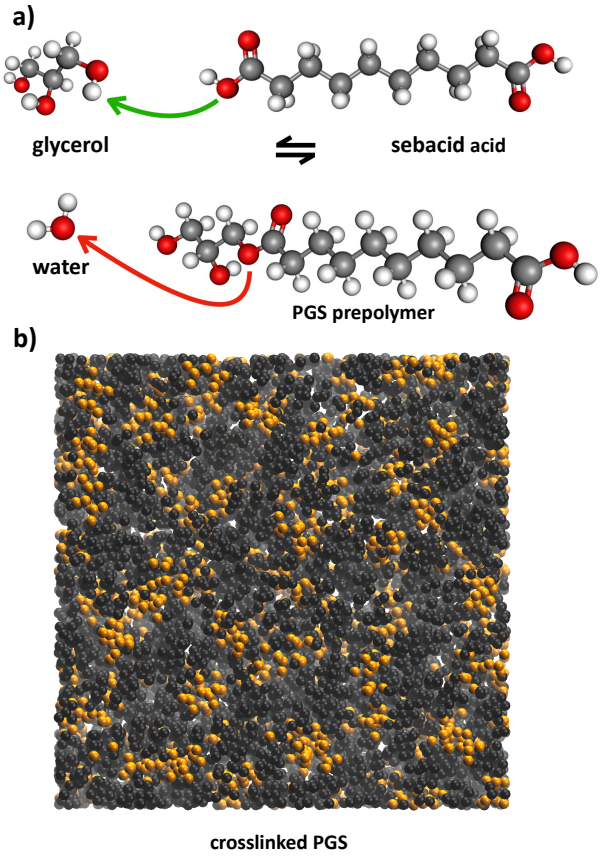

Figure 1: a) polycondensation of glycerol and sebacic acid molecules to yield the PGS prepolymer and b) a molecular representation of the crosslinked PGS polymer obtained with a 2:3 glycerol to sebacic acid ratio leading also to stoechiometry conditions for the OH and COOH functional groups. The glycerol atoms are represented in orange and sebacic acid atoms in black.

$$U(\lambda_i) = \lambda_i\, U_1 + (1 - \lambda_i)\, U_0 \quad (9)$$

where U_1 is the potential energy in the reference system denoted as ($\lambda = 1$). This is the initial state and U_1 considers all the interactions between the solid and liquid phases without any conversion. Since the perturbation consists of progressively removing the intermolecular interactions between the atoms of the solid and liquid phases, the target system ($\lambda = 0$) represents the final state in which these interactions become zero. U_0 only considers the interactions in the solid and liquid separated phases.

To promote overlaps between consecutive steps, the calculation of the work of adhesion W_{SL} between the two states (1) and (0) is split into N_w intermediate contiguous states or windows defined by a coupling constant λ_i and $w_{\mathrm{SL}}(\lambda_i)$.

$$W_{\mathrm{SL,FEP}} = \sum_{i=1}^{N_w} w_{\mathrm{SL}}(\lambda_i) = W^{(0)}_{\mathrm{SL,FEP}} - W^{(1)}_{\mathrm{SL,FEP}} \tag{10}$$

The perturbations can be performed in both directions (double-wide sampling) with N_w windows over the entire simulation. The different values of the coupling parameter are $\lambda_i = 1 - \frac{1}{N_w}(i-1)$ and $\lambda_i = 1 - \frac{1}{N_w}(i)$ in the forward and backward directions, respectively. In principle, for a reversible process, W_{SL} calculated in the forward direction with Eq (11) and backward direction with Eq (12) should be equal but of opposite sign. The difference between the two directions gives a lower-bound estimate of the error in the calculations and informs about the accuracy and convergence of the perturbation.

$$w^{\mathrm{forward}}_{\mathrm{SL,FEP}}(\lambda_i) = -\frac{1}{\beta\mathcal{A}} \sum_{i=1}^{N_w} \ln \left\langle \exp\left[-\beta\Big(U(\lambda_{i+1}) - U(\lambda_i)\Big)\right]\right\rangle_{\lambda_i} \tag{11}$$

$$w^{\mathrm{backward}}_{\mathrm{SL,FEP}}(\lambda_i) = -\frac{1}{\beta\mathcal{A}} \sum_{i=1}^{N_w} \ln \left\langle \exp\left[-\beta\Big(U(\lambda_{i-1}) - U(\lambda_i)\Big)\right]\right\rangle_{\lambda_i} \tag{12}$$

where $\mathcal{A}$ is the surface area of the solid and $U(\lambda_{i+1})$, $U(\lambda_i)$ and $U(\lambda_{i-1})$ are the the potential energies at λ_{i+1}, λ_i, λ_{i-1}, respectively. $\beta = \frac{1}{k_B T}$ where k_B is Boltzmann's constant and T the temperature. It is also possible to calculate the work of adhesion by using other approaches based on the concepts of Thermodynamic Integration (TI)[65] and Finite Difference Thermodynamic Integration (FDTI).[65] These methods calculate the derivative of U with respect to the coupling parameter λ as expressed in Eq.(13).

$$W_{\mathrm{SL,TI,FDTI}} = \frac{1}{\mathcal{A}} \int_1^0 \left\langle \frac{\partial U}{\partial \lambda} \right\rangle \mathrm{d}\lambda \tag{13}$$

The derivative of U with respect to λ is approximated by a finite difference in the TI formalism as defined in the following expressions of the forward and backward contributions.

$$\left\langle \frac{\partial U}{\partial \lambda} \right\rangle^{\mathrm{forward}}_{\mathrm{TI},\lambda_i} = \frac{\Big\langle U(\lambda_{i+1}) - U(\lambda_i) \Big\rangle}{\delta\lambda} \tag{14}$$

$$\left\langle \frac{\partial U}{\partial \lambda} \right\rangle^{\mathrm{backward}}_{\mathrm{TI},\lambda_i} = \frac{\Big\langle U(\lambda_{i-1}) - U(\lambda_i) \Big\rangle}{\delta\lambda} \tag{15}$$

The Finite Difference Thermodynamic Integration (FDTI) method calculates the derivative of U with respect to λ by using the perturbation method as

$$\left\langle \frac{\partial U}{\partial \lambda} \right\rangle^{\mathrm{forward}}_{\mathrm{FDTI},\lambda_i} = -\frac{1}{\beta}\frac{1}{\delta\lambda} \ln \left\langle \exp\left[-\beta\Big(U(\lambda_{i+1}) - U(\lambda_i)\Big)\right]\right\rangle_{\lambda_i} \tag{16}$$

$$\left\langle \frac{\partial U}{\partial \lambda} \right\rangle^{\mathrm{backward}}_{\mathrm{FDTI},\lambda_i} = -\frac{1}{\beta}\frac{1}{\delta\lambda} \ln \left\langle \exp\left[-\beta\Big(U(\lambda_{i-1}) - U(\lambda_i)\Big)\right]\right\rangle_{\lambda_i} \tag{17}$$

where $\lambda_{i\pm1} = \lambda_i \pm \delta\lambda$. The transformation from state (i) to state $(i+1)$ is achieved by changing the interactions between atoms of the solid phase and atoms of the liquid phase whose interactions are to be removed according to

$$\varepsilon_{SL}(\lambda_i) = \lambda_i\, \varepsilon_{SL} \tag{18}$$

where S and L represent the atoms of the solid (PGS) and liquid (water) phases, respectively. The removal of the interactions between atoms of S and L can lead to instabilities when the coupling parameter λ_i approaches 0. A solution[66] was to soften the Lennard-Jones potential by a soft core function[67] as

$$U_{\mathrm{LJ}}(r_{ij}, \lambda_i) = 4\,(\lambda_i)^n\, \varepsilon_{ij} \left[\frac{1}{\left(\alpha_{LJ}\,(1-\lambda_i)^2 + \left(\frac{r_{ij}}{\sigma_{ij}}\right)^6\right)^2} - \frac{1}{\alpha_{LJ}\,(1-\lambda_i)^2 + \left(\frac{r_{ij}}{\sigma_{ij}}\right)^6} \right] \tag{19}$$

where α_{LJ} was taken to 0.5. The electrostatic interactions were then modified by using a soft core at short distance as

$$U_{\text{elect}}(r_{ij},\lambda_i) = (\lambda_i)^n \frac{q_i\, q_j}{4\pi\,\epsilon_0 \left[\alpha_C(1-\lambda_i)^2 + r_{ij}^2\right]^{1/2}} \tag{20}$$

where α_C was taken to $10\,\text{Å}^2$ and n equal to 1. As λ_i is 1, the species to be considered in the perturbation interact through the full strength of the Lennard-Jones and Coulomb potentials. As λ_i approaches 0, the Lennard-Jones and Coulomb potentials are softened by soft-core interactions $\alpha_{LJ}(1-\lambda_i^2)$ and $\alpha_C(1-\lambda_i^2)$, respectively.

Formation of the crosslinked network of PGS

Various methods were designed to build a three dimensional network of crosslinked polymers by using molecular simulations such as the use of reactive forcefields[68] or coarse-grained simulations associated with a backmapping method.[69] We have recently developed a more straightforward method[46] based on the criteria of distances for bond creation. We define the degree of esterification as the percentage of esterified carboxyl groups to the total carboxyl groups in the simulation cell. In order to reach a high esterification ratio (above 90%[27]), the network is generated using a multistep algorithm[46] described in Figure 2. Since we want to simulate dry PGS, the production of water during the esterification reaction is prevented by removing the corresponding atoms from the reactants. As a consequence, during the esterification process, the alcohol Hs of the glycerol and the acid OHs of sebacic acid are absent. After 500 ps of equilibration, simulations were alternated between 50 ps in NPT and 50 ps in NVT statistical ensembles. Equilibration and NPT/NVT simulations were performed at 400 K and under a pressure of 1 bar with a timestep of 1 fs. A comprehensive description of the esterification algorithm can be found in ref. 46.

During the NVT simulations, van der Waals interactions between reactive sites (O of glycerol alcohols and C of sebacic acid carboxylic acids) were calculated by only the attractive

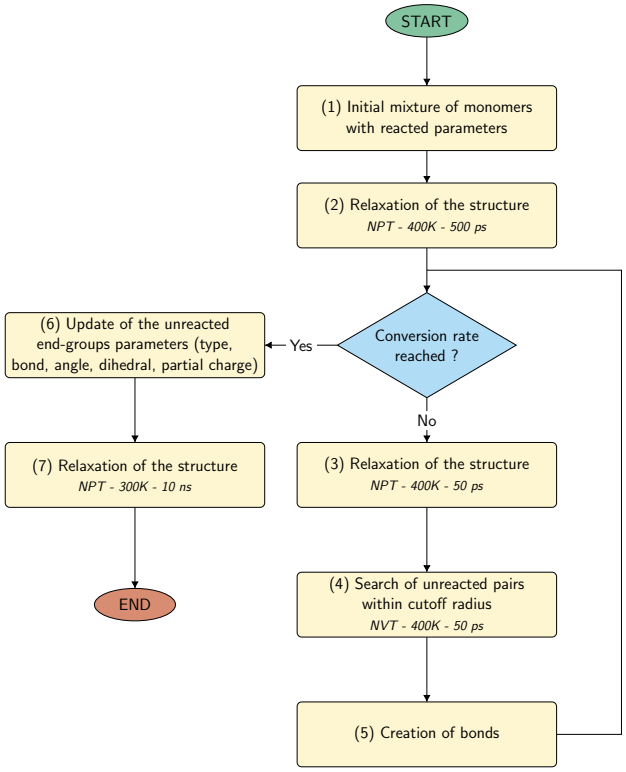

Figure 2: Multistep algorithm used to design the PGS at a given esterification degree. Adapted by removing a few steps and changing the simulation temperatures and reprinted in part with permission from Ref 46. Copyright 2022 American Chemical Society.

part of the Lennard-Jones potential. When reactive sites were closer than a defined cutoff, a bond was created between those atoms and a new cycle started. Sites which did not react were then functionalized back with the missing H and OH atoms and the network was then equilibrated at 300 K for 10 ns with 5×10^6 steps of 2 fs. For choosing the cutoff, the radial distribution function of reactive sites from monomers under reacted form at 400 K was computed. As the equilibrium distance between reactive sites was 3.36 Å, the value chosen for the cutoff needed to be smaller and was chosen as 1.25 times larger than the theoretical ester bondlength (1.327 Å) ie 1.6587 Å. For simulations involving surfaces, the same steps are followed replacing NPT ensemble by NVT with harmonic walls to confine molecules inside a slab.

In order to establish a comparison at different

esterification ratio ranging from 20 to 94 %, the system size was limited to 50 molecules of glycerol and 75 molecules of sebacic acid. To limit the error due to small system-sizes, five different systems of PGS or specimens were reticulated to the target esterification ratios.

Molecular dynamics (MD) simulations

Unless stated otherwise, all MD simulations were performed using the velocity-Verlet integrator with a Nosé-Hoover thermostat[70,71] at 300 K and 1 bar. The SHAKE algorithm[72] was used to constraint covalent bonds to hydrogen atoms. MD simulations in the NPT statistical ensemble[73] setting a pressure of 1 atm were performed by combining the hydrostatic equations of Martyna et al.[74] with the strain energy proposed by Parrinello and Rahman.[75] Temperature was imposed via a Langevin thermostat. Five different crosslinked PGS materials were used for each system. A specimen is a different initial configuration used in the polycondensation process. This means that the five specimens are independent configurations which correspond to the same degree of esterification. The molecular dynamics calculations were performed using the LAMMPS package.[76]

Results and discussions

Gel point

The gel point[77] corresponds to the presence of an infinite polymer network. From a molecular viewpoint, the gel point occurs when a single molecule covers the entire length of the simulation cell through the periodic conditions. At the molecular scale, the gel point of a network can be determined by tailoring the biggest cluster molecular mass, comparing the largest cluster molecular mass to the second largest cluster molecular mass or detecting the maximum of the weight average reduced molecular weight[78] (RMW). However, these methods are lacking precision[50] since they depend on the size of the system and are defined by changes in slope or by comparisons of sizes. With molecular dynamics systems, it is possible to determine exactly the point of formation of an infinite molecule by traversing along the molecule bonds and detecting a cycle that connects an atom to its own image through periodic boundaries. Using graph theory with python NetworkX package,[79] the percolation can be tailored by representing the system at the molecular level as a directed graph in which the atoms are the nodes and the bonds between atoms are the edges. Additionally, by defining the weight of each edge as the difference between the image flags of its source an target atoms, the Bellman-Ford algorithm can be used to detect negative cycles. An infinite molecule implies that the sum of weights along a self-connecting path crossing the box boundary is non-zero. The molecular mass of the first and second largest clusters along with the weight-averaged reduced molecular weight as a function of esterification degree are represented in Figure 3.

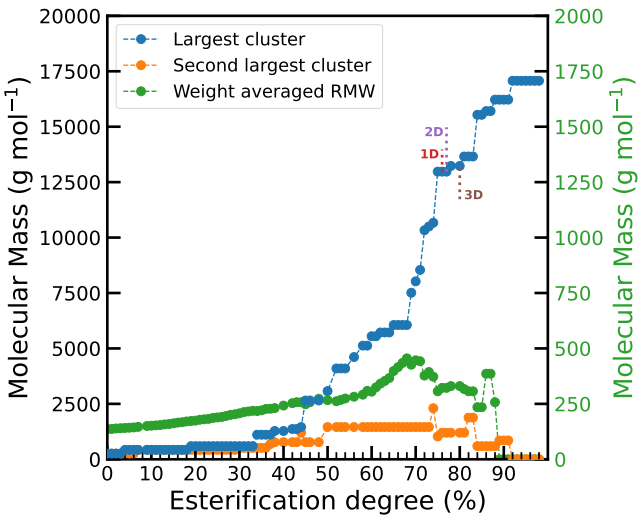

Figure 3: Molecular mass of the largest cluster (blue symbols), of the second largest cluster (orange symbols) and of the weight-averaged reduced molecular weight clusters (in green on the right-hand axis) as a function of the esterification degree. The percolation in zero, one, two and three dimensions is represented on the largest cluster metric by vertical lines 1D, 2D and 3D, respectively.

Concerning the polymer network of Figure

3, the largest cluster method shows an inflection point or gel point at about 75% whereas the reduced molecular weight (RMW) metric yield predicts a peak value identifying the gel point at 68%. The same calculations carried out over four different specimens give values of gel points ranging from 65 to 80%. By applying the Bellman-Ford algorithm[80] over the five polymer networks, we obtain an average effective percolation in the three directions of 73%. These results match very well with the theoretical predictions of 70%[77] and 83%[81] and confirm the quality of our algorithm and molecular model used for the building of the three dimensional PGS crosslinked network.

Density

Five specimens of PGS were used to calculate the density from MD simulations. The density of the PGS was calculated over the last five nanoseconds of the simulation of 10 ns. The five values of densities are represented in transparency in Figure 4 along with the average value and its standard deviations. We also report in Figure 4 the dependence of the density of the crosslinked PGS on the esterification degree.

First, we observe that the simulated density does not show any significant dependence on the degree of esterification within the sampling errors. This quasi-constant value of the density with the curing time has also been observed experimentally for an equimolar mixture of glycerol and sebacic acid.[10] More precisely, the weak decrease of the density of about 0.5% from the gel point can be explained by the increase of the number of covalent bonds that leads to a shrinkage of the network. Second, we obtain a good agreement with experiments showing a deviation of the order of 1%. Actually, an experimental density[27] of 1.106 g cm^{-3} was measured on a PGS with 2:3 ratio of glycerol to sebacic acid at 90% of esterification.

Glass transition temperature

The method used to compute the glass transition temperature (T_g) is based on the dilatometry principle.[46,82] The density decreases with increasing the temperature. The glass transition temperature (T_g) is then characterized by a break in this slope, showing a change in the relaxation speed of the PGS material when changing from viscous to glassy states. A Langevin thermostat in the NPT ensemble was used to calculate T_g with a timestep of 1 fs.

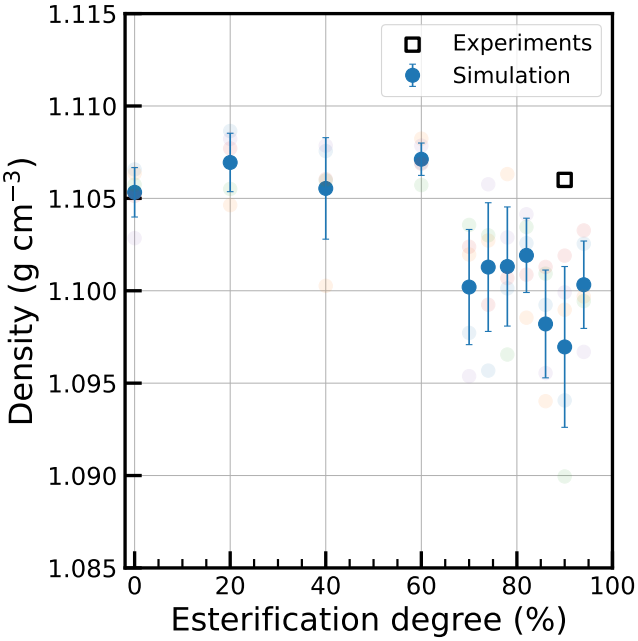

Figure 4: Density of a crosslinked PGS network as a function of the esterification degree. Transparent dots represent density values of each specimen while the blue dots indicate the mean value with its standard deviation. The experimental density is taken from ref. 27

After a ramp of 2 ns to heat the system from 300 K to 500 K, the system was relaxed at 500 K during 2 ns. By simulating the cooling of the system from 500 to 100 K at a rate of 20 K ns^{-1}, we report the evolution of the specific volume as a function of temperature in Figure 5 for the five specimens of PGS at 90% of esterification. After an equilibration period of 1 ns during which the temperature is gradually decreased by 20 K, the specific volume was averaged every 1 ps during additional 1 ns of acquisition at constant temperature. The specific volumes of each specimen are represented along with the average value and its standard deviation. Three linear fits based on the best mean R-squared were carried out on three re-

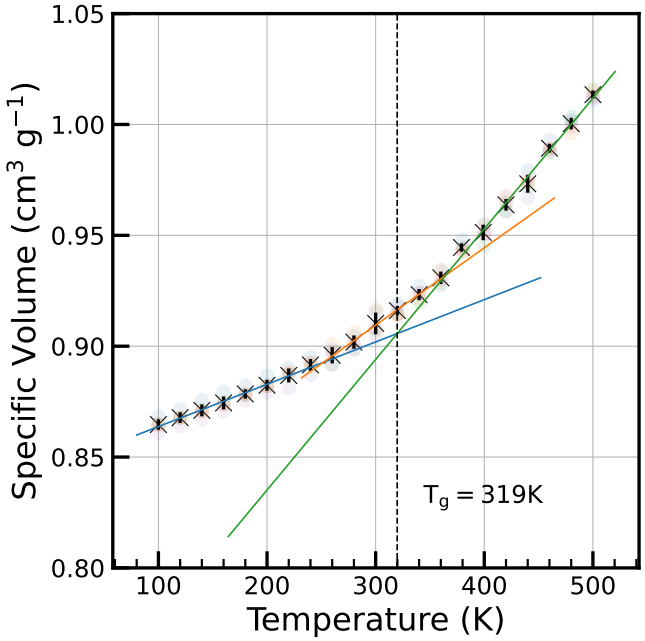

Figure 5: Specific volume of the PGS material with an esterification degree of 90% as a function of temperature during the cooling from 500 to 100 K. Transparent circles represent each of the five specimens. The mean values are the blacks crosses with error bars. The blue line corresponds to the glassy state, the orange line corresponds to the transitioning state and the green line corresponds to the viscous state. The intercept of the blue and green lines represented by the vertical dashed line is considered as the T_g value of the PGS material prior to any correction due to the fast cooling rate of molecular simulation.

gions delimiting the viscous state (green line), the glassy state (blue line) and the transitioning state (orange line). The glass transition temperature, defined as the intercept of the fits of the viscous and glassy states, is then equal to 319 K. The cooling rate applied in experiments[30,36] of 10 K min^{-1} is of several orders of magnitude slower than that used in molecular simulation. This means that we have to correct the simulated value by a contribution that takes into account both experimental and simulated cooling rates. This correction was estimated by using the Williams-Landel-Ferry (WLF) semi-empirical relation[83] that expresses the contribution to be added to the simulated T_g as

$$\Delta T_g = \frac{-C_2 \log\left(\frac{q_{\text{sim}}}{q_{\text{exp}}}\right)}{C_1 + \log\left(\frac{q_{\text{sim}}}{q_{\text{exp}}}\right)} \tag{21}$$

where q_{sim} and q_{exp} are equal to 20 K ns^{-1} and 10 K min^{-1} and universal values[82] $C_1 = 17.44$ K and $C_2 = 51.6$ K. ΔT_g was then equal to -90 K. It means that the simulated T_g of PGS is then estimated at 239 K which falls in the 236..268 K range of experimental temperatures.[8,24,30,36,37]

We report in Figure 6 the glass transition temperature calculated over five different specimens as a function of the degree of esterification. We also add for comparison the experimental values of T_g obtained at different curing times.[30] We used the work of Li et al.[29] to link the curing time to the degree of esterification. First, we observe that the simulated values of T_g match very well with the experimental ones within the statistical fluctuations with maximum deviations of 9%. Second, Figure 6 establishes that increasing the degree of esterification does not change the glass transition temperature of PGS in agreement with recent experiments.[30,31]

Work of adhesion and water contact angle

We now turn our attention to the hydrophilicity of PGS by investigating the interactions between the PGS and water. We calculated the work of adhesion of PGS-water interface by doing alchemical transformations consisting of turning off the intermolecular interactions between water molecules and PGS material. The transformation was divided into 41 windows each of which was composed of an equilibration period of 100 ps and an acquisition phase of 100 ps in the NVT statistical ensemble. PGS-water systems were built by placing a cubic box of 1049 water molecules of 35 Å on the top of the PGS surface. The values of the cumulative values of the work of adhesion $w_{\text{SL}}(\lambda)$ are given in Figure 7 for the FEP, TI and FDTI approaches with $\Delta\lambda = 0.025$ and $\delta\lambda = 2 \times 10^{-3}$.

First, we check that the interaction between

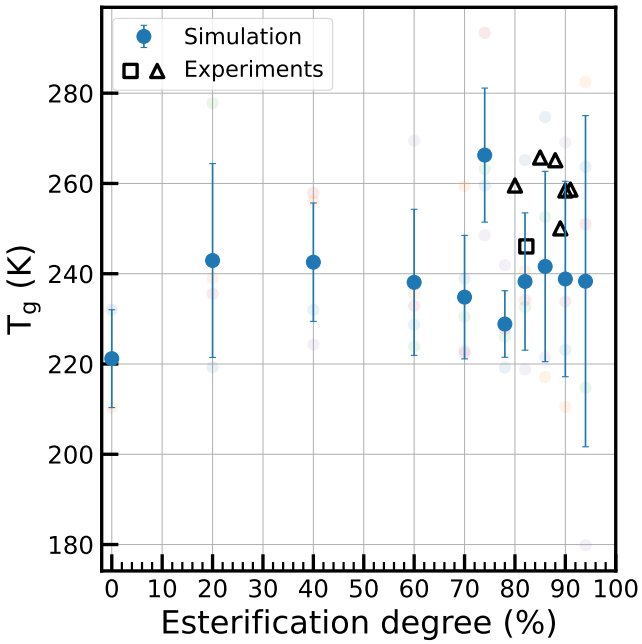

Figure 6: Simulated values of glass transition temperatures (T_g) as a function of the degree of esterification. The average temperatures were calculated over five specimens with a cooling rate of $20\,\mathrm{K\,ns^{-1}}$. The solid blue circles represent the averages whereas the transparent symbols refer to the temperatures of each of five specimens. The experimental values of T_g are taken from ref. 36 (□) and ref. 30(△).

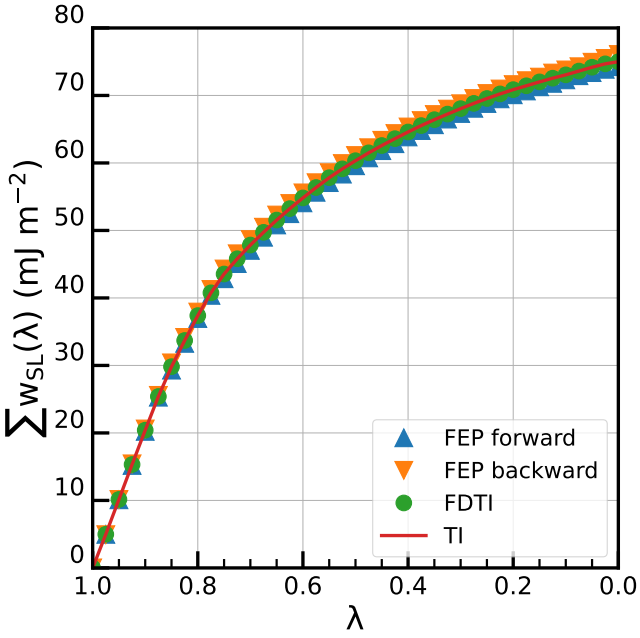

Figure 7: Cumulative $w_{SL}(\lambda)$ work of adhesion values as a function of the coupling parameter λ calculated during the transformation. The FEP results were given for the two opposite directions. For FEP in the reverse directions, we took the absolute value of $w_{SL}(\lambda)$ to represent them with the same scale. The TI and FDTI results were averaged over both directions. The calculation was performed on a PGS with a degree of esterification of 90%.

water and PGS is favorable from a free energy viewpoint since the transformation consisting of turning off the interactions led to a positive free energy. Second, Figure 7 shows that the FEP data calculated in the forward and backward directions collapse together on the scale of the graph and that the FDTI and TI free energy contributions averaged on both directions arrange themselves between the direct and reverse points of FEP. More precisely, the value of W_{SL} is given by the last value ($\lambda = 0$) of curves given in Figure 7. For an esterification degree of 90%, the FEP technique gives 76 and $-78\,\mathrm{mJ\,m^{-2}}$ for the forward and backward directions, respectively whereas TI and FDTI methodologies yield $75\,\mathrm{mJ\,m^{-2}}$ for W_{SL} averaged over both directions. These characteristics confirm the validity of the calculation in terms of an efficient sampling of the phase space and reversibility of the thermodynamic transformation. We plot in Figure 8 the work of adhesion W_{SL} as a function of the esterification degree. The values of W_{SL} were averaged on 5 specimens and on FEP, FDTI and TI methods.

Figure 8 shows that the work of adhesion decreases almost linearly with the degree of esterification indicating that the strength of the interaction between PGS and water decreases with the increase of esterified carboxyl groups indicating that the hydrophilicity of the resulting PGS material is weakened with the degree of esterification. For a more direct comparison with the experiment, we propose to calculate the water contact angle through the work of adhesion. Indeed, experiments usually measure the Young contact angle θ, which is related to different surface tensions through the Young's equation.[84–86]

$$\gamma_{SL} - \gamma_{SV} + \gamma_{LV}\cos\theta = 0 \qquad (22)$$

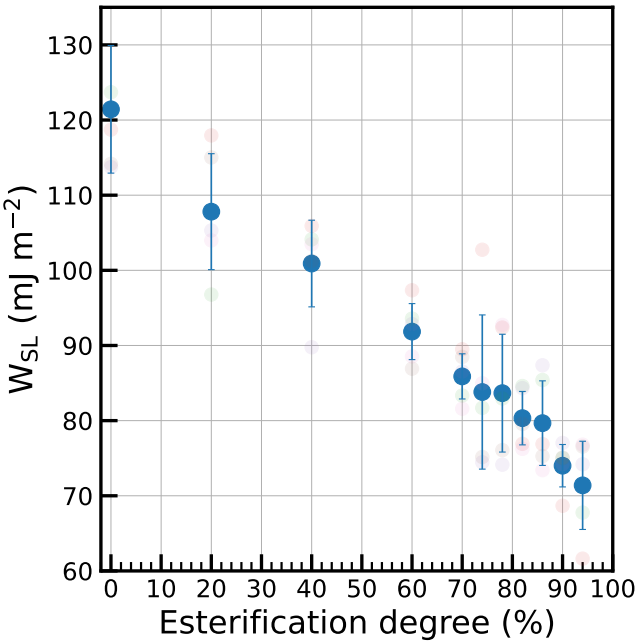

Figure 8: Work of adhesion (W_{SL}) between PGS and water as a function of the degree of esterification. The solid blue circles correspond to the average carried out over the FEP, TI and FDTI methods and over five different initial configurations whose values are represented with transparent symbols.

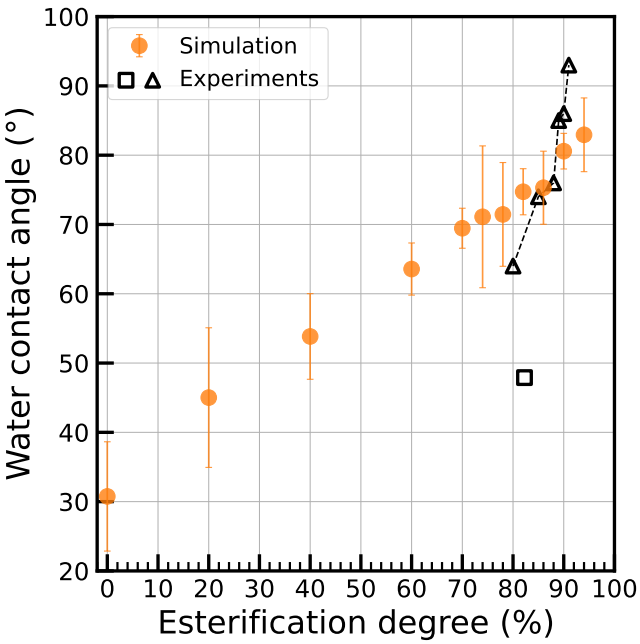

Figure 9: Water contact angle calculated from the work of adhesion at different esterification degrees. The experimental values of θ were taken from ref. 36 (□) and ref. 30(△). We used the work of Li et al.[29] to link the curing time to the degree of esterification.

By replacing $\gamma_{SV} - \gamma_{SL}$ by $\gamma_{LV}\cos\theta$ by using Eq.(8), we obtain the following expression relating W_{SL} and θ as

$$W_{SL} = \gamma_{LV}\,(1 + \cos\theta) \qquad (23)$$

By using Eq.(23), we report in Figure 9 the water contact angle of PGS as a function of the degree of esterification. We observe that this water contact angle increases almost linearly from 30° to 82° as the degree of esterification changes from 0 to 94%. The value of the surface tension of the liquid-vapor interface of water γ_{LV} was taken to 63.6 mN m^{-1} at 300 K with the SPC/E model.[87]

We check that the order of magnitude of the water contact angle and linearity of the dependence of γ on the degree of esterification are very well reproduced by our molecular simulations establishing the performance of our molecular models for predicting the interfacial properties of PGS. However, we observe that the available experimental contact angle show an higher slope compared to simulated contact angles which can be partly explained by the correlation we make between the curing time and the esterification degree. Nevertheless, molecular simulation can help rationalize some experiments, as the determination of the water contact angle is subject to operating conditions for both the measurement of θ and the design of PGS material. In the next section, we propose to describe the PGS-water interface at the molecular level in order to explain the decrease of the hydrophilicity with the degree of esterification.

Atomistic description of the PGS-water interface

We calculate the number of hydrogen bonds between PGS material and water molecules by considering the following criteria:[88] water molecules and PGS atoms are chosen as being hydrogen bonded only if the distance (O-H..O) between the donor and acceptor is less than 2.5 Å and simultaneously the angle O-H..O is greater than 150°. This analysis was performed

on the last 500 ps of an acquisition phase of 1 ns. The number of hydrogen bond was averaged over the five independent PGS materials for a given degree of esterification. The dependence of the work of adhesion on the strength of the hydrogen bond network at the interface is given in Figure 10.

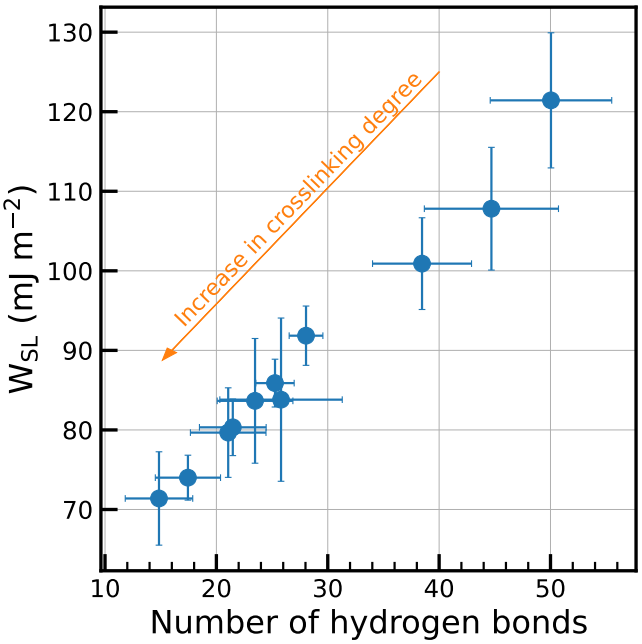

Figure 10: Work of adhesion of the PGS-water system as a function of the number of hydrogen bonds between water molecules and PGS. The criteria used to select an hydrogen bond have been taken from ref. 88.

Figure 10 shows a direct correlation between W_{SL} and the number of hydrogen bonds. In other terms, the greater the W_{SL}, the smaller the water contact angle and the stronger the network of hydrogen bonds at the interface. Within the range of degree of esterification investigated here, we observe a decrease of the number of hydrogen bonds of 42% for a water contact angle increasing from 30° to 82°. Clearly, molecular simulations establish here a correlation between the hydrophilicity of PGS at different esterification degrees with the number of hydrogen bonds with water. This is an interesting result for the interpretation of experiments.

Figure 11a shows the atomistic density profiles of atoms of PGS and water molecules along the z-direction normal to the surface for a crosslinked PGS at 90%. This analysis was performed on the last 50 ns of a NPT simulation of 200 ns. By focusing on the interfacial region, Figure 11a shows that the density profile of water molecules decreases from the bulk value to zero over a z-region of about 7 Å. We also observe an overlap interfacial region between PGS atoms and water molecules extending over 5 Å. To complete this view of the interface and to avoid the impact of the smoothing on the density profile due to a local surface roughness, we calculate the intrinsic density profiles[89–91] of PGS and water (see Figure 11b) by considering the following expression

$$\rho(z') = \left\langle \frac{1}{A}\sum_{i=1}^{N}\delta(z'-z_i)\right\rangle = \left\langle \frac{1}{A}\sum_{i=1}^{N}\delta(z-z_i+\xi(x_i,y_i))\right\rangle \tag{24}$$

where ξ is the instantaneous position of the surface and x_i and y_i are the atomic coordinates in the plane parallel to the PGS surface. The calculation of $\xi(x_i, y_i)$ is done by moving down a (x, y) grid of fictitious spheres along the z axis, starting in the water region. Once a surface atom i is detected at a given distance from the probe sphere, $\xi(x_i, y_i)$ is set to the current z coordinate of the surface atom.

Clearly, these intrinsic profiles show an interfacial region of non-overlap between water and PGS with an ordering of water molecules close to the PGS surface. It means that over the time scale of the simulation, we do not observe absorption of water in PGS provided that the water absorption capacity of PGS remains limited.[30] Finally, the profile of the average $\langle\cos\theta\rangle$ where θ is defined as the angle between the vector normal to the PGS surface and the water molecular dipole vector is shown in Figure 11c as a function of the z-direction. As $\langle\cos\theta\rangle \approx 0$ in the bulk water phase far from the surface, this implies no preferred orientations for water molecules. When approaching the PGS surface, we observe some peaks at $\langle\cos\theta\rangle \approx 0.15$ and $\langle\cos\theta\rangle \approx -0.2$ indicating that the water molecules tend to adopt specific orientations parallel to the PGS surface. These parallel orientations of water molecules in the adsorption layer is the result of a trade-off between main-

taining hydrogen bonds with water molecules and developing hydrogen bonds with PGS.

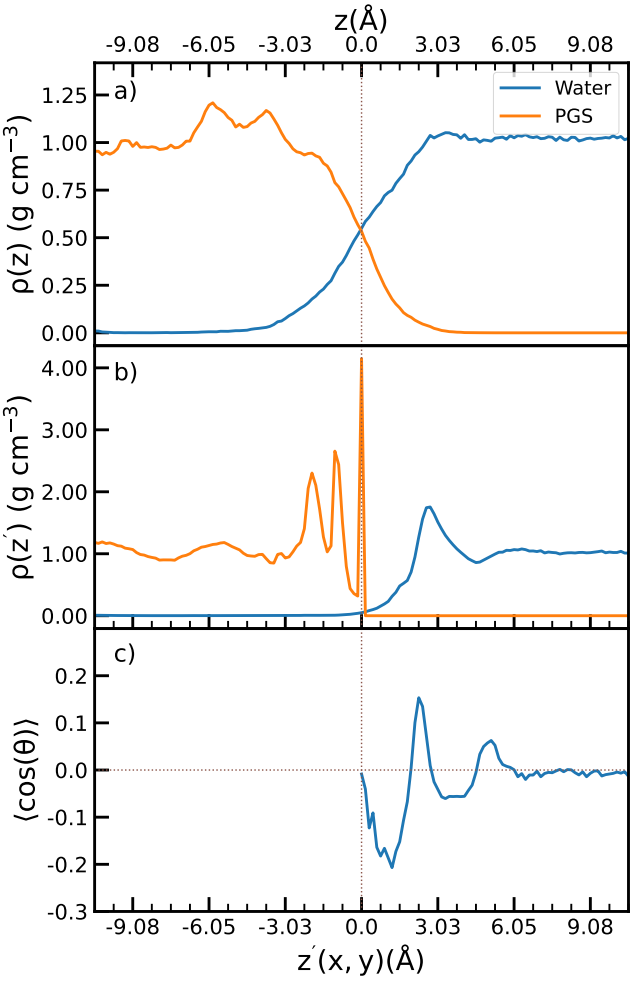

Figure 11: a) Density profiles and b) intrinsic density profiles of water and PGS atoms for a degree of esterification of 90%. The origin of z in b) and c) is chosen as the last atom of the solid phase. No water molecule actually penetrated inside the PGS slab. c) Average $\langle \cos\theta \rangle$ along the z-direction where θ is the angle between the molecular dipole vector of water and the vector normal to the PGS surface. Some degree of orientation ordering can be observed in the first water layers. These profiles were calculated on a single simulation but no significant changes were observed between the profiles of different specimens.

Conclusions

We carried out molecular simulations with the aim of providing a better description of the PGS-water interface. The algorithm for building the crosslinked network of PGS was shown to be efficient to reach a high degree of esterification but also to estimate the gel point of the structure. The density of the crosslinked PGS was correctly reproduced with respect to experiments and no clear dependence of the density on the degree of esterification was deduced from molecular simulations. The determination of the glass transition temperature showed a good agreement with experiments. The degree of esterification was shown not to affect this thermal property. The investigation of the PGS-water interface was carried out through the calculation of the work of adhesion and water contact angle. An important result was to show that the water contact angle increases almost linearly with the degree of esterification as recently established by experiments. In addition, the values of water contact angle agreed very well with the corresponding experimental properties. Interestingly, we established for the first time at the molecular scale, a direct correlation between the water contact angle and the number of hydrogen bonds between PGS and water molecules. We completed this study by the description of the interfacial region in terms of specific arrangement and orientations of water molecules along the direction normal to the PGS surface.

This molecular simulation study showed that it was possible to predict macroscopic properties for PGS materials comparable to experiments while providing a microscopic view of the interfacial region. One of the main advantage of molecular simulations is to control the degree of esterification and then be in a position to investigate its impact on target properties. This could also complement the interpretation of experiments.

On the basis of this study, we aim to examine the interaction between drugs and PGS in the context of controlled drug delivery in order to better evaluate the different energy contributions involved in this process.

Acknowledgement This work was performed in SimatLab, a joint public-private laboratory dedicated to the modeling of poly-

mer materials. This laboratory is supported by Michelin, Clermont Auvergne University (UCA), CHU Clermont-Ferrand and CNRS. We are grateful to the Mésocentre Clermont Auvergne University for providing computing and storage resources. This work was performed using HPC resources from GENCI-IDRIS (Grant AD010913369R1).

References

(1) SESTOFT, L. An Evaluation of Biochemical Aspects of Intravenous Fructose, Sorbitol and Xylitol Administration In Man. *Acta Anaesthesiol. Scand.* **1985**, *29*, 19–29.

(2) Bruggeman, J. P.; de Bruin, B.-J.; Bettinger, C. J.; Langer, R. Biodegradable Poly (Polyol Sebacate) Polymers. *Biomater.* **2008**, *29*, 4726–4735.

(3) Wang, Y.; Ameer, G. A.; Sheppard, B. J.; Langer, R. A Tough Biodegradable Elastomer. *Nat. Biotechnol.* **2002**, *20*, 602–606.

(4) Godinho, B.; Gama, N.; Ferreira, A. Different Methods Of Synthesizing Poly(Glycerol Sebacate) (PGS): A Review. *Front. Bioeng. Biotechnol.* **2022**, *10*, 1033827.

(5) Vogt, L.; Ruther, F.; Salehi, S.; Boccaccini, A. R. Poly(Glycerol Sebacate) in Biomedical Applications—A Review of the Recent Literature. *Adv. Healthcare Mater.* **2021**, *10*, 2002026.

(6) Liu, Q.; Tian, M.; Shi, R.; Zhang, L.; Chen, D.; Tian, W. Structure and Properties of Thermoplastic Poly (Glycerol Sebacate) Elastomers Originating From Prepolymers With Different Molecular Weights. *J. Appl. Polym. Sci.* **2007**, *104*, 1131–1137.

(7) Sundback, C. A.; Shyu, J. Y.; Wang, Y.; Faquin, W. C.; Langer, R. S.; Vacanti, J. P.; Hadlock, T. A. Biocompatibility Analysis Of Poly (Glycerol Sebacate) As A Nerve Guide Material. *Biomater.* **2005**, *26*, 5454–5464.

(8) Cai, W.; Liu, L. Shape-Memory Effect Of Poly (Glycerol–Sebacate) Elastomer. *Mater. Lett.* **2008**, *62*, 2171–2173.

(9) Wang, Y.; Kim, Y. M.; Langer, R. In Vivo Degradation Characteristics Of Poly(Glycerol Sebacate). *J. Biomed. Mater. Res.* **2003**, *66A*, 192–197.

(10) Pomerantseva, I.; Krebs, N.; Hart, A.; Neville, C. M.; Huang, A. Y.; Sundback, C. A. Degradation Behavior Of Poly(Glycerol Sebacate). *J. Biomed. Mater. Res. A* **2009**, *91A*, 1038–1047.

(11) Sun, Z.-J.; Chen, C.; Sun, M.-Z.; Ai, C.-H.; Lu, X.-L.; Zheng, Y.-F.; Yang, B.-F.; Dong, D.-L. The Application Of Poly (Glycerol–Sebacate) As Biodegradable Drug Carrier. *Biomater.* **2009**, *30*, 5209–5214.

(12) Yang, B.; Lv, W.; Deng, Y. Drug Loaded Poly(Glycerol Sebacate) As A Local Drug Delivery System For The Treatment Of Periodontal Disease. *RSC Adv.* **2017**, *7*, 37426–37435.

(13) Massironi, A.; Marzorati, S.; Marinelli, A.; Toccaceli, M.; Gazzotti, S.; Ortenzi, M. A.; Maggioni, D.; Petroni, K.; Verotta, L. Synthesis and Characterization of Curcumin-Loaded Nanoparticles of Poly(Glycerol Sebacate): A Novel Highly Stable Anticancer System. *Molecules* **2022**, *27*, 6997.

(14) Chen, Q.-Z.; Bismarck, A.; Hansen, U.; Junaid, S.; Tran, M. Q.; Harding, S. E.; Ali, N. N.; Boccaccini, A. R. Characterisation Of A Soft Elastomer Poly(Glycerol Sebacate) Designed To Match The Mechanical Properties Of Myocardial Tissue. *Biomater.* **2008**, *29*, 47–57.

(15) Masoumi, N.; Jean, A.; Zugates, J. T.; Johnson, K. L.; Engelmayr, G. C. Laser Microfabricated Poly(Glycerol Sebacate)

Scaffolds For Heart Valve Tissue Engineering. *J. Biomed. Mater. Res.* **2013**, *101A*, 104–114.

(16) Liang, B.; Shi, Q.; Xu, J.; Chai, Y.-M.; Xu, J.-G. Poly (Glycerol Sebacate)-Based Bio-Artificial Multiporous Matrix for Bone Regeneration. *Front. Chem.* **2020**, *8*, 603577.

(17) Rai, R.; Tallawi, M.; Grigore, A.; Boccaccini, A. R. Synthesis, Properties And Biomedical Applications Of Poly(Glycerol Sebacate) (PGS): A Review. *Prog. Polym. Sci.* **2012**, *37*, 1051–1078.

(18) Loh, X. J.; Abdul Karim, A.; Owh, C. Poly(Glycerol Sebacate) Biomaterial: Synthesis And Biomedical Applications. *J. Mater. Chem. B* **2015**, *3*, 7641–7652.

(19) Piszko, P.; Kryszak, B.; Piszko, A.; Szustakiewicz, K. Brief Review on Poly(glycerol sebacate) As an Emerging Polyester in Biomedical Application: Structure, Properties And Modifications. *Polym. Med.* **2021**, *51*, 43–50.

(20) Aydin, H. M.; Salimi, K.; Rzayev, Z. M. O.; Pişkin, E. Microwave-Assisted Rapid Synthesis Of Poly(Glycerol-Sebacate) Elastomers. *Biomater. Sci.* **2013**, *1*, 503.

(21) Perin, G. B.; Felisberti, M. I. Enzymatic Synthesis of Poly(glycerol sebacate): Kinetics, Chain Growth, and Branching Behavior. *Macromolecules* **2020**, *53*, 7925–7935.

(22) Li, X.; Hong, A. T.-L.; Naskar, N.; Chung, H.-J. Criteria for Quick and Consistent Synthesis of Poly(glycerol sebacate) for Tailored Mechanical Properties. *Biomacromolecules* **2015**, *16*, 1525–1533.

(23) Lau, C. C.; Bayazit, M. K.; Knowles, J. C.; Tang, J. Tailoring Degree Of Esterification And Branching Of Poly(Glycerol Sebacate) By Energy Efficient Microwave Irradiation. *Polym. Chem.* **2017**, *8*, 3937–3947.

(24) Conejero-García, Á.; Gimeno, H. R.; Sáez, Y. M.; Vilariño-Feltrer, G.; Ortuño-Lizarán, I.; Vallés-Lluch, A. Correlating Synthesis Parameters With Physicochemical Properties Of Poly(Glycerol Sebacate). *Eur. Polym. J.* **2017**, *87*, 406–419.

(25) Gadomska-Gajadhur, A.; Wrzecionek, M.; Matyszczak, G.; Pietowski, P.; Wiecław, M.; Ruśkowski, P. Optimization Of Poly(Glycerol Sebacate) Synthesis For Biomedical Purposes With The Design of Experiments. *Org. Process Res. Dev.* **2018**, *22*, 1793–1800.

(26) Kim, M. J.; Hwang, M. Y.; Kim, J.; Chung, D. J. Biodegradable and Elastomeric Poly(glycerol sebacate) as a Coating Material for Nitinol Bare Stent. *Biomed Res. Int.* **2014**, *2014*, 1–7.

(27) Nagata, M.; Machida, T.; Sakai, W.; Tsutsumi, N. Synthesis, Characterization, And Enzymatic Degradation Of Network Aliphatic Copolyesters. *J. Polym. Sci., Part A: Polym. Chem.* **1999**, *37*, 2005–2011.

(28) Kafouris, D.; Kossivas, F.; Constantinides, C.; Nguyen, N. Q.; Wesdemiotis, C.; Patrickios, C. S. Biosourced Amphiphilic Degradable Elastomers of Poly(glycerol sebacate): Synthesis and Network and Oligomer Characterization. *Macromolecules* **2013**, *46*, 622–630.

(29) Li, X.; Hong, A. T.-L.; Naskar, N.; Chung, H.-J. Criteria for Quick and Consistent Synthesis Of Poly (Glycerol Sebacate) for Tailored Mechanical Properties. *Biomacromolecules* **2015**, *16*, 1525–1533.

(30) Wu, Z.; Jin, K.; Wang, L.; Fan, Y. Effect of Curing Time On The Mechanical Properties Of Poly (Glycerol Sebacate). *J. Appl. Polym. Sci.* **2023**, *140*, e53700.

(31) Jaafar, I. H.; Ammar, M. M.; Jedlicka, S. S.; Pearson, R. A.; Coulter, J. P. Spectroscopic Evaluation,

Thermal, and Thermomechanical Characterization of Poly (Glycerol-Sebacate) With Variations In Curing Temperatures And Durations. *J. Mat. Sci.* **2010**, *45*, 2525–2529.

(32) Yoon, S.; Chen, B. Elastomeric and PH-Responsive Hydrogels Based On Direct Crosslinking Of The Poly (Glycerol Sebacate) Pre-Polymer And Gelatin. *Polym. Chem.* **2018**, *9*, 3727–3740.

(33) Saudi, A.; Rafienia, M.; Zargar Kharazi, A.; Salehi, H.; Zarrabi, A.; Karevan, M. Design And Fabrication of Poly (Glycerol Sebacate)-Based Fibers For Neural Tissue Engineering: Synthesis, Electrospinning, And Characterization. *Polym. Adv. Technol.* **2019**, *30*, 1427–1440.

(34) Heng, P. W. S. Controlled Release Drug Delivery Systems. *Pharm. Dev. Technol.* **2018**, *23*, 833–833.

(35) Adepu, S.; Ramakrishna, S. Controlled Drug Delivery Systems: Current Status and Future Directions. *Molecules* **2021**, *26*, 5905.

(36) Liu, Q.; Tian, M.; Ding, T.; Shi, R.; Zhang, L. Preparation And Characterization Of A Biodegradable Polyester Elastomer With Thermal Processing Abilities. *J. Appl. Polym. Sci.* **2005**, *98*, 2033–2041.

(37) Rai, R.; Tallawi, M.; Roether, J. A.; Detsch, R.; Barbani, N.; Rosellini, E.; Kaschta, J.; Schubert, D. W.; Boccaccini, A. R. Sterilization Effects on The Physical Properties And Cytotoxicity Of Poly (Glycerol Sebacate). *Mater. Lett.* **2013**, *105*, 32–35.

(38) Vogt, L.; Rivera, L. R.; Liverani, L.; Piegat, A.; El Fray, M.; Boccaccini, A. R. Poly (ε-Caprolactone)/Poly (Glycerol Sebacate) Electrospun Scaffolds For Cardiac Tissue Engineering Using Benign Solvents. *Mater. Sci. Eng. C .* **2019**, *103*, 109712.

(39) Law, K.-Y. Definitions For Hydrophilicity, Hydrophobicity, and Superhydrophobicity: Getting The Basics Right. *J. Phys. Chem. Lett.* **2014**, *5*, 686–688.

(40) Rostamian, M.; Kalaee, M. R.; Dehkordi, S. R.; Panahi-Sarmad, M.; Tirgar, M.; Goodarzi, V. Design and Characterization Of Poly (Glycerol-Sebacate)-Co-Poly (Caprolactone)(PGS-co-PCL) and Its Nanocomposites As Novel Biomaterials: The Promising Candidate For Soft Tissue Engineering. *Eur. Polym. J* **2020**, *138*, 109985.

(41) Lau, C.; Al Qaysi, M.; Owji, N.; Bayazit, M.; Xie, J.; Knowles, J.; Tang, J. Advanced Biocomposites of Poly (Glycerol Sebacate) and β-Tricalcium Phosphate By In Situ Microwave Synthesis For Bioapplication. *Mater. Today Adv.* **2020**, *5*, 100023.

(42) Aghajan, M. H.; Panahi-Sarmad, M.; Alikarami, N.; Shojaei, S.; Saeidi, A.; Khonakdar, H. A.; Shahrousvan, M.; Goodarzi, V. Using Solvent-Free Approach For Preparing Innovative Biopolymer Nanocomposites Based On PGS/Gelatin. *Eur. Polym. J* **2020**, *131*, 109720.

(43) Piszko, P.; Kryszak, B.; Szustakiewicz, K. Influence of Cross-linking Time On Physico-Chemical And Mechanical Properties of Bulk Poly (Glycerol Sebacate). *Acta Bioeng. Biomech.* **2022**, *24*, 85–93.

(44) Risley, B. B.; Ding, X.; Chen, Y.; Miller, P. G.; Wang, Y. Citrate Crosslinked Poly (Glycerol Sebacate) With Tunable Elastomeric Properties. *Macromol. Biosc.* **2021**, *21*, 2000301.

(45) Allen, M. P.; Tildesley, D. J. *Computer Simulation of Liquids*; Oxford: Clarendon Press, 1987.

(46) Orselly, M.; Devemy, J.; Bouvet-Marchand, A.; Dequidt, A.; Loubat, C.; Malfreyt, P. Molecular Simulations of

Thermomechanical Properties of Epoxy-Amine Resins. *ACS Omega* **2022**, *7*, 30040–30050.

(47) Orselly, M.; Devémy, J.; Bouvet-Marchand, A.; Dequidt, A.; Loubat, C.; Malfreyt, P. Molecular Interactions At The Metal–Liquid Interfaces. *J. Chem. Phys.* **2022**, *156*, 234705.

(48) Orselly, M.; Richard, C.; Devémy, J.; Bouvet-Marchand, A.; Dequidt, A.; Loubat, C.; Malfreyt, P. Impact of The Force Field on the Calculation of Density and Surface Tension of Epoxy–Resins. *J. Phys. Chem. B* **2023**, *127*, 2617–2628.

(49) Xu, B.; Li, Y.; Zhu, C.; Cook, W. D.; Forsythe, J.; Chen, Q. Fabrication, Mechanical Properties and Cytocompatibility Of Elastomeric Nanofibrous Mats Of Poly (Glycerol Sebacate). *Eur. Polym. J.* **2015**, *64*, 79–92.

(50) Livraghi, M.; Höllring, K.; Wick, C. R.; Smith, D. M.; Smith, A.-S. An Exact Algorithm to Detect the Percolation Transition in Molecular Dynamics Simulations of Cross-Linking Polymer Networks. *J. Chem. Theory Comput.* **2021**, *17*, 6449–6457.

(51) Jorgensen, W. L.; Maxwell, D. S.; Tirado-Rives, J. Development and Testing of the OPLS All-Atom Force Field on Conformational Energetics and Properties of Organic Liquids. *J. Am. Chem. Soc.* **1996**, *118*, 11225–11236.

(52) Jorgensen, W. L.; Tirado-Rives, J. Potential Energy Functions for Atomic-Level Simulations of Water and Organic and Biomolecular Systems. *Proc. Natl. Acad. Sci. U. S. A.* **2005**, *102*, 6665–6670.

(53) Robertson, M.; Tirado-Rives, J.; Jorgensen, W. Improved Peptide and Protein Torsional Energetics with the OPLS-AA Forcefield. *J. Chem. Theory Comput.* **2015**, *11*, 3499–3509.

(54) Eastwood, J. W.; Hockney, R. W.; Lawrence, D. N. P3M3DP - Rhe 3-Dimensional Periodic Particle-Particle-Particle-Mesh Program. *Comput. Phys. Commun.* **1980**, *19*, 215–261.

(55) Berendsen, H. J. C.; Grigera, J. R.; Straatsma, T. P. The Missing Term in Effective Pair Potentials. *J. Phys. Chem.* **1987**, *91*, 6269–6271.

(56) Lorentz, H. A. Ueber die Anwendung des Satzes vom Virial in der kinetischen Theorie der Gase. *Ann. Phys.* **1881**, *12*, 127–136.

(57) Berthelot, D. C. R. Sur le Mélange des Gaz. *Hebd. Acad. Sci.* **1898**, *126*, 1703–1855.

(58) Vassetti, D.; Pagliai, M.; Procacci, P. Assessment of GAFF2 and OPLS-AA General Force Fields In Combination With The Water Models TIP3P, SPCE, and OPC3 For The Solvation Free Energy of Druglike Organic Molecules. *J. Chem. Theory Comput.* **2019**, *15*, 1983–1995.

(59) Kadaoluwa Pathirannahalage, S. P.; Meftahi, N.; Elbourne, A.; Weiss, A. C.; McConville, C. F.; Padua, A.; Winkler, D. A.; Costa Gomes, M.; Greaves, T. L.; Le, T. C.; Besford, Q. A.; Christofferson, A. J. Systematic Comparison of The Structural And Dynamic Properties of Commonly Used Water Models For Molecular Dynamics Simulations. *J. Chem. Inf. Model.* **2021**, *61*, 4521–4536.

(60) Malfreyt, P. Calculation of The Surface Tension of Planar Interfaces By Molecular Simulations: From Lennard-Jones Fluids To Binary Mixtures. *Mol. Simul.* **2014**, *40*, 106–114.

(61) Israelachvili, J. N. *Intermolecular and Surfaces Forces*, 3rd ed.; Academic Press: New-York, 2011.

(62) Zwanzig, R. W. High Temperature Equation of State by a Perturbation Method. *J. Chem. Phys.* **1954**, *22*, 1420–1426.

(63) Mezei, M.; Beveridge, D. L. Free Energy Simulations. *Ann. N. Y. Acad. Sci.* **1986**, *482*, 1–23.

(64) Ghoufi, A.; Malfreyt, P. Entropy and Enthalpy Calculations From Perturbation and Integration Thermodynamics Methods Using Molecular Dynamics Simulations: Applications to the Calculation of Hydration and Association Thermodynamic Properties. *Mol. Phys.* **2006**, *104*, 2929–2943.

(65) Chipot, C., Pohorille, A., Eds. *Free Energy Calculations: Theory and Applications in Chemistry and Biology*; Springer Series in Chemical Physics 86; Springer: Berlin ; New York, 2007.

(66) Beutler, T. C.; Mark, A. E.; van Schaik, R. C.; Gerber, P. R.; van Gunsteren, W. F. Avoiding Singularities and Numerical Instabilities in Free Energy Calculations Based on Molecular Simulations. *Chem. Phys. Lett.* **1994**, *222*, 529–539.

(67) Devémy, J.; Dequidt, A.; Malfreyt, P. A Consistent Thermodynamic Characterization of the Adsorption Process through the Calculation of Free Energy Contributions. *J. Phys. Chem. B* **2023**, *127*, 5360–5370.

(68) Yilmaz, D. E.; Woodward, W. H.; van Duin, A. C. T. Machine Learning-Assisted Hybrid ReaxFF Simulations. *J. Chem. Theory Comput.* **2021**, *17*, 6705–6712.

(69) Komarov, P. V.; Yu-Tsung, C.; Shih-Ming, C.; Khalatur, P. G.; Reineker, P. Highly Cross-Linked Epoxy Resins: An Atomistic Molecular Dynamics Simulation Combined with a Mapping/Reverse Mapping Procedure. *Macromolecules* **2007**, *40*, 8104–8113.

(70) Nosé, S. A Molecular Dynamics Method for Simulations In the Canonical Ensemble. *Mol. Phys.* **1984**, *52*, 255–268.

(71) Hoover, W. G. Canonical dynamics: Equilibrium phase-space distributions. *Phys. Rev. A* **1985**, *31*, 1695.

(72) Ryckaert, J.-P.; Ciccotti, G.; Berendsen, H. J. Numerical Integration of The Cartesian Equations Of Motion Of A System With Constraints: Molecular Dynamics Of n-Alkanes. *J. Comp. Phys.* **1977**, *23*, 327–341.

(73) Melchionna, S.; Ciccotti, G.; Lee Holian, B. Hoover NPT Dynamics For Systems Varying In Shape And Size. *Mol. Phys.* **1993**, *78*, 533–544.

(74) Martyna, G. J.; Tobias, D. J.; Klein, M. L. Constant pressure molecular dynamics algorithms. *J. Chem. Phys.* **1994**, *101*, 4177–4189.

(75) Parrinello, M.; Rahman, A. Polymorphic Transitions In Single Crystals: A New Molecular Dynamics Method. *J. Appl. Phys.* **1981**, *52*, 7182–7190.

(76) Plimpton, S. Fast Parallel Algorithms For Short-Range Molecular Dynamics. *J. Comp. Phys.* **1995**, *117*, 1–19.

(77) Flory, P. J. Molecular Size Distribution in Three Dimensional Polymers. I. Gelation [1]. *J. Am. Chem. Soc.* **1941**, *63*, 3083–3090.

(78) Patil, S. U.; Shah, S. P.; Olaya, M. N.; Deshpande, P. P.; Maiaru, M.; Odegard, G. M. Molecular Dynamics Study To Predict Thermo-Mechanical Properties Of Dgebf/Detda Epoxy As A Function Of Crosslinking Density. *arXiv preprint arXiv:2108.00933* **2021**,

(79) Hagberg, A. A.; Schult, D. A.; Swart, P. J. Exploring Network Structure, Dynamics, and Function using NetworkX. Proceedings of the 7th Python in Science Conference. Pasadena, CA USA, 2008; pp 11 – 15.

(80) Bang-Jensen, J.; Gutin, G. Z. *Digraphs: Theory, Algorithms And Applications*; Springer Science & Business Media, 2008.

(81) Carothers, W. H. Polymers and Polyfunctionality. *Trans. Faraday Soc.* **1936**, *32*, 39–49.

(82) Soldera, A.; Metatla, N. Glass Transition Of Polymers: Atomistic Simulation Versus Experiments. *Phys. Rev. E* **2006**, *74*, 061803.

(83) Williams, M. L.; Landel, R. F.; Ferry, J. D. The Temperature Dependence Of Relaxation Mechanisms In Amorphous Polymers And Other Glass-Forming Liquids. *J. Am. Chem. Soc.* **1955**, *77*, 3701–3707.

(84) Young, T. An Essay On The Cohesion Of Fluids. *Philos. Trans. R. Soc. London* **1805**, *95*, 65.

(85) Marmur, A. Soft Contact: Measurement And Interpretation Of Contact Angles. *Soft Matter* **2006**, *2*, 12–17.

(86) Bormashenko, E. Physics Of Solid–Liquid Interfaces: From The Young Equation To The Superhydrophobicity. *Low Temp. Phys.* **2016**, *42*, 622–635.

(87) Vega, C.; De Miguel, E. Surface Tension Of The Most Popular Models Of Water By Using The Test-Area Simulation Method. *J. Chem. Phys.* **2007**, *126*, 154707.

(88) Luzar, A.; Chandler, D. Effect of Environment on Hydrogen Bond Dynamics in Liquid Water. *Phys. Rev. Lett.* **1996**, *76*, 928–931.

(89) Partay, L. B.; Hantal, G.; Jedlovsky, P.; Vincze, A.; Horvai, G. A New Method for Determining the Interfacial Molecules and Characterizing the Surface Roughness in Computer Simulations. Application to the Liquid–Vapor Interface of Water. *J. Comput. Chem.* **2008**, *29*, 945–956.

(90) Jorge, M.; Hantal, G.; Jedlovszky, P.; Cordeiro, M. N. D. S. A Critical Assessment of Methods for the Intrinsic Analysis of Liquid Interfaces: 2. Density Profiles. *J. Phys. Chem. C* **2010**, *114*, 18656–18663.

(91) Lapshin, D. N.; Jorge, M.; Campbell, E. E. B.; Sarkisov, L. On Competitive Gas Adsorption and Absorption Phenomena in Thin Films of Ionic Liquids. *J. Mater. Chem. A* **2020**, *8*, 11781–11799.

TOC Graphic